

## Metal-oxide-based nanocomposites comprising advanced gas sensing properties

This article has been downloaded from IOPscience. Please scroll down to see the full text article.

2012 J. Phys.: Conf. Ser. 345 012029

(<http://iopscience.iop.org/1742-6596/345/1/012029>)

View [the table of contents for this issue](#), or go to the [journal homepage](#) for more

Download details:

IP Address: 130.209.6.41

The article was downloaded on 05/04/2012 at 14:30

Please note that [terms and conditions apply](#).

## Metal-oxide-based nanocomposites comprising advanced gas sensing properties

A A Ponomareva<sup>1,2</sup>, V A Moshnikov<sup>1</sup>, D Glöb<sup>3</sup>, A Delan<sup>2</sup>, A Kleiner<sup>2</sup>,  
G Suchanek<sup>2</sup>

<sup>1</sup>St. Petersburg State Electrotechnical University (LETI), 197376 St. Petersburg, Russia

<sup>2</sup>TU Dresden, Solid State Electronics Laboratory, 01062 Dresden, Germany

<sup>3</sup>Fraunhofer Institute for Electron Beam and Plasma Processing (FEP), 01277 Dresden, Germany

E-mail: ap\_k@inbox.ru, Gunnar.Suchanek@tu-dresden.de

**Abstract.** Using the sol-gel technique, nanocomposite SiO<sub>2</sub>-SnO<sub>2</sub> thin films comprising a designed hierarchical pore structure were prepared on cost-efficient oxidized silicon substrates. These films exhibit advanced gas sensing properties both for reducing gases and oxygen due to an efficient analyte transport by mesopores.

### 1. Introduction

Gas sensitivity of metal oxide gas sensors increases rapidly when the dimensions of oxide sensing materials become comparable or smaller than the typical thickness of the electron depletion layer [1]. Therefore, nanosized materials exhibit outstanding properties in sensor application, particularly low operation temperature and high sensitivity, attributed to their large surface area to volume ratio.

Hierarchical structures are higher dimensional structures composed of many, lower dimensional building blocks. Because they are generally larger than the individual nanostructures, their van der Waals attraction is relatively weak. On the other hand, hierarchical microstructures provide an effective gas diffusion path via well aligned mesoporous structures without sacrificing a high surface area [2]. Consequently, they exhibit high gas sensitivity and fast gas response. Hierarchical nanostructures for gas sensors were prepared by vapour phase growth, hydrothermal or hydrothermal/solvothermal reactions [2], by electrospinning and subsequent oxygen plasma etching [3], by ultrasonic spray pyrolysis [4], by flame-spray-pyrolysis [5, 6], and by pulsed laser deposition techniques [7]. Well defined hierarchical pore structures were prepared by sol-gel method in alkoxy-derived silica systems [8] as well as in aluminium salt solutions [9] utilizing a phase separation mechanism as a pore forming principle. Recently, one of our laboratories has applied this approach for the fabrication of SnO<sub>2</sub>-SiO<sub>2</sub> composites comprising hierarchical macro-, meso- and micropores (according to IUPAC notation [10]). This minimises the build up of thermal stresses during sensor fabrication and, therefore, improves adhesion. Moreover, our technology is based on inexpensive precursors such as SnCl<sub>2</sub> and tetraethylorthosilicate (TEOS). In the first case, advantages compared to alkoxides are besides the precursor costs a reduced sensitivity of the precursor to heat, moisture and light, and an improved time stability of the sol against the increase in viscosity. On the other hand, the presence of Cl<sup>-</sup> increases the gelling time.

In this work, we investigate gas sensing properties of sol-gel deposited nanocrystalline SnO<sub>2</sub>-SiO<sub>2</sub> composites in relation to their microstructure and demonstrate gas sensitivities at the state-of-art level.

### 2. Experimental

Nanocrystalline SnO<sub>2</sub>-SiO<sub>2</sub> thin films comprising a hierarchical pore structure were fabricated using a polymeric sol-gel process. Tin (II) chloride dihydrate SnCl<sub>2</sub>•2H<sub>2</sub>O (M = 225.63 g/mol) was used as a tin precursor and tetraethylorthosilicate (TEOS) C<sub>8</sub>H<sub>20</sub>O<sub>4</sub>Si as a silica source (table 1). The solutions

were aged 24 h at room temperature and spin-coated onto oxidized silicon wafers without an adhesion promoter. The films were calcined at about 550°C in air for 5 minutes by transferring the wafer into a hot furnace. Cooling down was performed in the furnace within 12 to 14 hours.

**Table 1.** Solvent and chemical reagent ratio used for sol-gel nanocomposite SiO<sub>2</sub>-SnO<sub>2</sub> thin film deposition.

Composition* (Run number)	Solvent	Volume of solvent, ml	Weight of SnCl <sub>2</sub> ·2H <sub>2</sub> O, g	Volume of TEOS, μl
20%SiO <sub>2</sub> -80%SnO <sub>2</sub>	ethanol	10	0.242	60
20%SiO <sub>2</sub> -80%SnO <sub>2</sub>	<i>n</i> -butanol	10	0.154	28.7
10%SiO <sub>2</sub> -90%SnO <sub>2</sub>	<i>n</i> -butanol	10	0.173	19.1
100% SnO <sub>2</sub>	<i>n</i> -butanol	10	0.193	-

\* Percentages are in molar %

Composition analysis was performed by means of X-ray photoelectron spectroscopy (XPS) using MgK<sub>α</sub> (1253.6 eV) radiation in the vacuum chamber of a Physical Electronics PHI 5702 electron spectrometer. The surface composition was evaluated by calculating the peak areas of high-resolution XP spectra. The signal was calibrated referring to the C1s hydrocarbon signal at a binding energy of 285 eV. In order to clean the sample from carbon residues and adsorbed at the surface gases, Ar<sup>+</sup> sputter cleaning ( $E_{kin} = 4$  keV) was carried out removing an about 1.4 nm thick surface layer in two minutes. After argon ion bombardment, the C1s peak disappeared. In these cases XPS peaks were referred to the O1s signal at 531.15 eV. Microstructure of the deposited porous SnO<sub>2</sub>-SiO<sub>2</sub> films was investigated by atomic force microscopy (AFM) using an NTEGRA Thermo scanning probe microscope (NT-MDT, Zelenograd, Russia). Tapping mode imaging was performed in air using silicon cantilevers (Type NSG01, NDT-MDT, Moscow, Russia). AFM provides already a digitized image of 256x256 pixels suitable for numerical evaluation. Following an industrial standard for specifying the indication of surface texture of optical elements, especially its high spatial frequency errors (roughness) [11], an isotropic, one-dimensional power spectral density function  $PSD(k)$  where  $k$  is the wavevector (the spatial frequency in reciprocal space), of the surface topography was calculated. The two-dimensional AFM image was averaged over the profiles traced in fast scan direction using the Open Source Software Gwyddion 2.21 [12]. This allows reducing noise due to instrument drift appearing more pronounced in the slow scan direction. Moreover, the averaging over 256 scans is approximately equivalent to the integration of the two-dimensional PSD over the slow scan direction [13]. The specific surface area (SSA) was determined by means of the Brunauer, Emmett and Teller (BET) method with nitrogen adsorption using a Sorbi-N4.1 instrument (ZAO META, Novosibirsk, Russia). UV-VIS optical properties of the films were investigated in the wavelength range of 300 to 2000 nm with steps of 2 nm by absolute reflectance and transmittance measurements in a two-beam spectrophotometer (Lambda 950, PerkinElmer, USA).

Sensor structures were prepared using film deposited onto oxidized silicon substrates with *n*-butanol as a solvent. Nickel-chrome and gold layer of a thickness of 10 and 35 nm, respectively, were evaporated onto the SnO<sub>2</sub>-SiO<sub>2</sub> thin films. Thereby, the Ni-Cr layer serves for adhesion improvement. The patterned by a copper contact mask electrode layers formed 0.5 and 0.4 mm wide interdigital electrodes. Gas sensing experiments were carried out by using nitrogen (reference gas) and 1.5 vol.% hydrogen in nitrogen or oxygen provided by a computer controlled gas flow system. The purity of all gases was  $\geq 99.999$  Vol. %. The total gas flow was kept constant at 90 sccm. A gas sensor area of about 3.5 mm<sup>2</sup> on the silicon wafer was heated using a small platinum heater. The measurement setup is described in detail elsewhere [14]. Sensitivity to ethanol was determined in a computer controlled measurement setup described in [15]. Dry air dried was used as reference gas.

### 3. Results and discussion

XPS indicated a Si/(Si+Sn) ratio of about 0.27 at the surface (X-ray penetration depth about 5 nm) of both as-deposited and sputter-cleaned samples synthesized with a ratio Si/(Si+Sn) = 0.2. Carbon was present on the surface of as-deposited films by an amount of 22.5 %. Carbon disappeared after sputter cleaning. The higher silicon fraction obtained by XPS is probably caused by pores throughout the film with sizes larger than the film thickness of about 60 nm. Therefore, in the following Si/(Si+Sn) ratios based on the ratio in the solution are given. The Sn3d<sub>5/2</sub> peak appeared at 487.2 eV at slightly higher value than that of bulk SnO<sub>2</sub> (486.6 eV) indicating that tin is in the tetravalent state. The Sn3d<sub>5/2</sub> peak position did not change after sputter cleaning. The O1s peak was deconvoluted into two ones, a peak assigned to SiO<sub>2</sub> at 532.4 eV and a SnO<sub>2</sub> related one at 531.1 eV. Their peak area ratio was 0.2713 for the sputter cleaned sample in good agreement with the Si/(Si+Sn) determined from the XPS peak areas of the cations. In the Cl2p<sub>3/2</sub> region, no appreciable peak could be observed in the sample.

Optical properties of the SiO<sub>2</sub>-SnO<sub>2</sub> nanocomposites were already reported in [16]. Films deposited using *n*-butanol as solvent exhibit an optical band gap of about 4 eV. The larger compared to bulk SnO<sub>2</sub> (3.62 eV) band gap is attributed to the contribution of the quantum size effect [17, 18, 19] observable also in ultrathin films [20]. In our case, the band gap value of about 4 eV corresponds to a crystallite size of about 5 nm [17]. The optical band gap of films using ethanol as solvent was about 3.4 eV. All films were strongly disordered with an Urbach tail characteristic energy of 0.50 to 0.75 eV making a reliable determination of the optical gap difficult. Therefore, we have also determined the isoabsorption gap  $E_{04}$  at an absorption coefficient of  $\alpha = 10^4 \text{ cm}^{-1}$  yielding an optical gap of 4.51 and 3.95 eV for *n*-butanol and ethanol solvents, respectively.

The evaluation of the microstructure of hierarchical structures is challenging because of they span multiple length scales from the molecular to the macroscopic level. In our case, intrinsic film features are mostly pronounced in the range 10-100 nm making AFM a proper choice for microstructure characterization. The obtained by AFM surface topography can give qualitative insight into film formation processes such as cluster aggregation, pore formation, ordering etc.

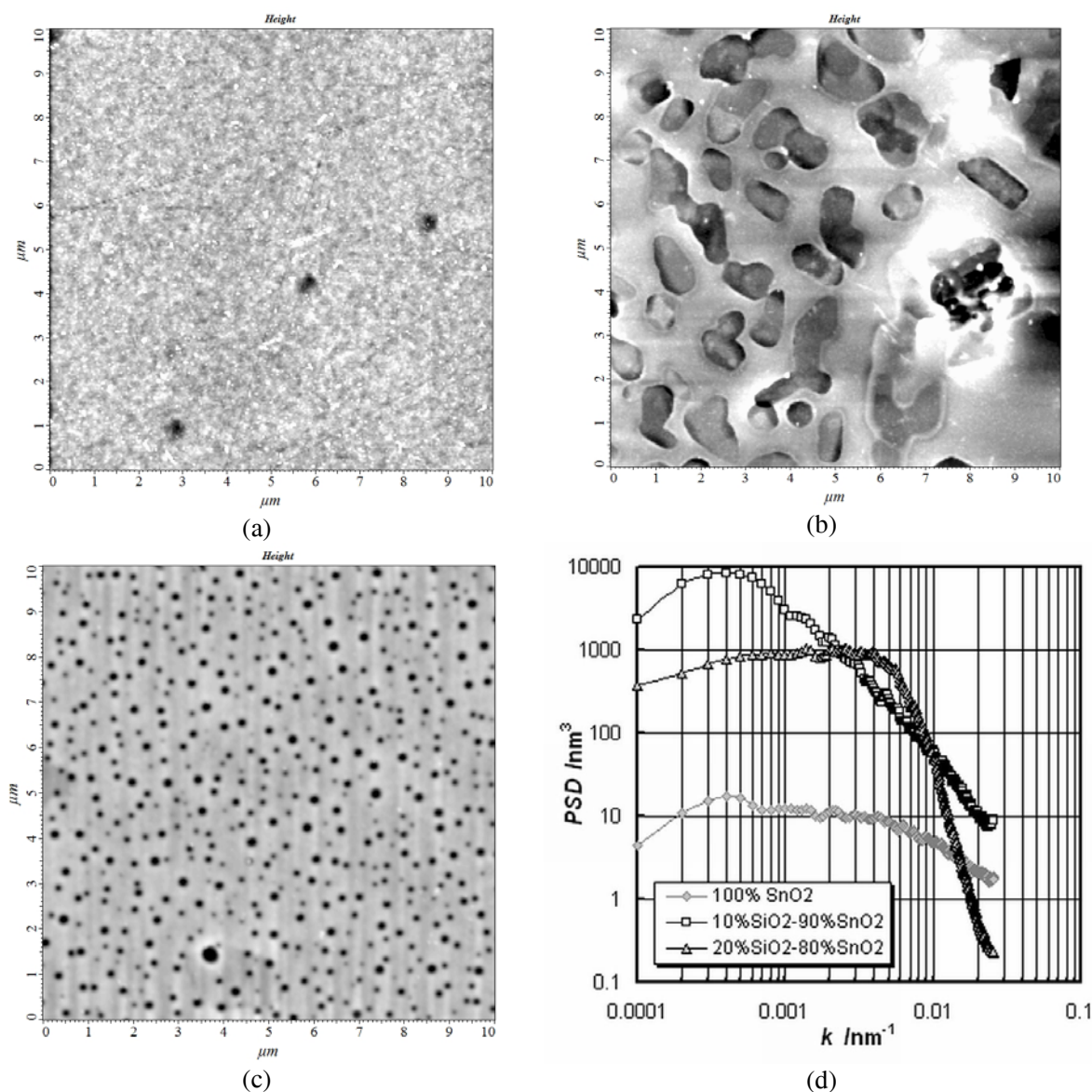
Surface texture is characterized by the height of its peaks, the depths of its valleys and the distances that separate them. The calculation of the PSD function by Fourier decomposition of the digitized AFM image into spatial frequencies takes into account the statistical correlations between the different surface points and hence it gives a more general description than the RMS surface roughness alone. Thus, the PSD identifies wavelengths of features that contribute to the surface structure. The one-dimensional PSD considered in this work is representative of a homogeneous and isotropic surface.

Figure 1 shows the surface texture of sol-gel processed SnO<sub>2</sub> film and SiO<sub>2</sub>-SnO<sub>2</sub> nanocomposites fabricated using *n*-butanol as solvent and the derived from AFM images PSDs. Practically no porosity was observed in the smooth films (RMS surface roughness about 0.9 nm) prepared without TEOS addition (Fig. 1a). The 10 at% SiO<sub>2</sub>-90 at% SnO<sub>2</sub> sample exhibits the largest porosity with a three-dimensional film structure (Fig. 1b). This related to the fact that TEOS is known to favour the formation of three-dimensional network of linked oxide particles in the gel leading to a proper pore structure in the annealed composites [21]. The surface of 10 at% SiO<sub>2</sub>-90 at% SnO<sub>2</sub> films is significantly roughened in the whole region of spatial wavelengths compared to SnO<sub>2</sub> films deposited by the same procedure without adding TEOS to the solution. The most pronounced feature size of 10 at% SiO<sub>2</sub>-90 at% SnO<sub>2</sub> films equals to 1.25  $\mu\text{m}$  (Fig. 1d). Note, that an increase of the PSD by two orders of magnitude corresponds to an increase of the RMS surface roughness  $R_{RMS}$  by one order of magnitude according to

$$R_{RMS} = \sqrt{\int_{k_1}^{k_2} PSD(k) dk} \quad (1)$$

where the reciprocal values of  $k_1$  and  $k_2$  determine the spatial wavelength bandwidth of the roughness measurement. The sample with 20 at% silica fraction had a decreased again roughness with circular pores of a broad size distribution (Fig. 1c). Spatial wavelengths below 250 nm are strongly attenuated giving evidence of a smoother surface at the nanometer level. The SSA of this film amounted to 87.21

$\text{m}^2/\text{g}$  yielding an average pore size of about 10 nm. SSA and average pore size are in good agreement with the values of similar films investigated in [22]. On the other hand, it has to be mentioned that these nanopores known to enhance gas sensitivity [23] cannot be imaged by our AFM device.



**Figure 1.** AFM-images of sol-gel layers: a – 100 at% SnO<sub>2</sub>; b – 10 at% SiO<sub>2</sub> – 90 at% SnO<sub>2</sub>; c – 20 at% SiO<sub>2</sub> – 80 at% SnO<sub>2</sub>, d – power spectral density of the images in figures a-c.

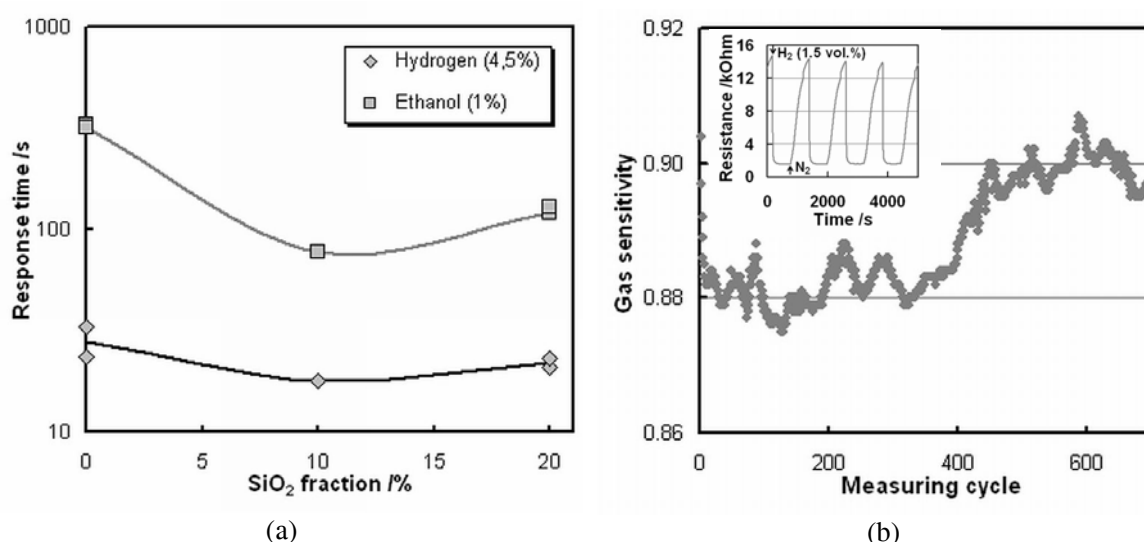
Selected results of gas sensitivity measurements at 200°C are summarized in table 2. Preliminary values of hydrogen gas sensitivity were already reported in [24]. The highest gas sensitivities were achieved by the sensor with 10 at% silica fraction possessing the highest porosity.

Figure 2a shows the response time of hydrogen and ethanol sensors in dependence on nanocomposite silica fraction. The quickest response was obtained for 10 at% silica fraction providing a high three-dimensional porosity. Thereby, the impact of porosity on response time is more pronounced for larger gas molecules. This gives evidence that sensor response time is limited by the analyte transport in mesopores. The response time exhibits the typical dependence on the gas

concentration, i.e., an increase of the response time with decreasing of gas concentration (not shown in figures) [24, 25, 26].

**Table 2.** Gas sensitivity of ( $S=\Delta R/R_{air}$ ) of SiO<sub>2</sub>-SnO<sub>2</sub> nanocomposite thin film sensors in dependence on analyte gas and gas concentration.

Nanocomposite	Gas sensitivity for the following gas concentration				
	H <sub>2</sub> 4500 ppm	H <sub>2</sub> 15000 ppm	C <sub>2</sub> H <sub>5</sub> OH 1000 ppm	O <sub>2</sub> 61500 ppm	O <sub>2</sub> 100000ppm
100 at% SnO <sub>2</sub>	0.38	0.48	0.29	0.32	0.43
10 at% SiO <sub>2</sub> -90 at% SnO <sub>2</sub>	0.85	0.93	0.71	1.40	2.00
20 at% SiO <sub>2</sub> -80 at% SnO <sub>2</sub>	0.76	0.86	0.47	0.96	1.56



**Figure 2.** Response time to hydrogen and ethanol in dependence on silica fraction of the nanocomposite (a) and gas sensitivity to hydrogen (1.5 vol.%) in dependence on measuring cycle number (b), all data measured at a temperature of 200°C.

In order to test long-term stability, seven hundred measuring cycles of hydrogen sensing were carried out. No degradation of hydrogen sensitivity was observed (Fig. 2b). Therefore, the fabricated in gas sensors are capable to overcome sensor drift and missing long-term stability known for state-of-art nanosized SnO<sub>2</sub> gas sensors [27, 28]. Longer term investigations are in progress now.

### Conclusions

SiO<sub>2</sub>-SnO<sub>2</sub> nanocomposites comprising a hierarchical pore structure were fabricated using tin(II) chloride dihydrate SnCl<sub>2</sub>•2H<sub>2</sub>O as a tin source and TEOS as a silicon source. In order to achieve advanced gas sensing properties, the porous film structure was optimized by varying the silica fraction of the nanocomposite. For the optimized composition of 10 at%SiO<sub>2</sub>-90 at%SnO<sub>2</sub>, mesopores provide an efficient analyte transport decreasing sensor response and recovery times. These sol-gel deposited SiO<sub>2</sub>-SnO<sub>2</sub> nanocomposites are promising materials for advanced metal oxide gas sensors.

### Acknowledgements

This work was supported by contracts 16.740.11.0211, P399 and P2279 of the Federal Target Program “Scientific and Scientific-Pedagogical Personnel of Innovative Russia for the period 2009-2013”, and by the Erasmus Mundus External Co-operation Window Programme of the European Union (A.P.).

**References**

- [1] Xu Ch, Tamaki J, Miura N and Yamazoe N 1991 *Sensors and Actuators B* **3** 147
- [2] Lee J-H 2009 *Sensors and Actuators B* **140** 319
- [3] Zhang Y, Li J, An G and He X 2010 *Sensors and Actuators B* **144** 43
- [4] Firooza A A, Hyodo T, Mahjoub A R, Khodadadi A A and Shimizu Y 2010 *Sensors and Actuators B* **147** 554
- [5] Tricoli A, Graf M and Pratsinis S E 2008 *Advanced Functional Materials* **18** 1969
- [6] Qu Y, Xue T, Zhong X, Lin Y C, Liao L, Choi J and Duan X 2010 *Advanced Functional Materials* **20** 3005
- [7] Chen Z, Pan D, Zhao B, Ding G, Jiao Z, Wu M, Shek C-H, Wu L C M and Lai J K L 2010 *ASNNano* **4** 1202
- [8] Nakanishi K 1997 *Journal of Porous Materials* **4** 67
- [9] Tokudome Y, Fujita K, Nakanishi K, Miura K and Hirao K 2007 *Chem. Mater.* **19** 3393
- [10] Rouquerol J, Avnir D, Fairbridge C W, Everett D H, Haynes J M, Pernicone N, Ramsay J D F, Sing K S W and Unger K K 1994 *Pure & Appl. Chem.* **66** 1739
- [11] Draft DIN ISO 10110-8:2010, 2011-03-07
- [12] Gwyddion – data analysis software: <http://gwyddion.net>
- [13] Marx E, Malik I J, Strausser Y E, Bristow T, Poduje N and Stover J C 2002 *J. Vac. Sci. Technol. B* **20** 31
- [14] Delan A, Karuppasamy A and Schultheiß E 2009 *Plasma Processes and Polymers* **6** S731
- [15] Gracheva I E, Maksimov A I, Moshnikov V A and Plekh M E 2008 *Instruments and Experimental Techniques* **51** 462-465
- [16] Ponomareva A A, Moshnikov V A and Suchanec G 2011 *Technical Physics Letters* **37** 892-895
- [17] Gu F, Wang S F, Lü M K, Zhou G J, Xu D and Yuan D R 2004 *J. Phys. Chem. B* **108** 8119
- [18] Yu B, Zhu C and Gan F 1997 *Optical Materials* **7** 15
- [19] Gu F, Wang S F, Lu M K, Cheng X F, Liu S W, Zhou G J, Xu D and Yuan D R 2004 *J. Cryst. Growth* **262** 182
- [20] Gaidi M, Hajjaji A, Smirani R, Bessais B and El Khakani M A 2010 *J. Appl. Phys.* **108** 063537
- [21] Blanco E, Esquivias L, R Litran R, Pinero M, Ramirez-del-Solar M and de la Rosa-Fox N 1999 *Sonogels and Derived Materials Appl. Organometal. Chem.* **13** 399
- [22] Gracheva I E, Moshnikov V A, Karpova S S and Maraeva E V 2011 *J. Phys: Conf. Ser.* **291** 012017
- [23] Yang J, Hidajat K and Kawi S 2008 *Materials Letters* **62** 1441
- [24] Ponomareva A A, Moshnikov V A and Suchanec G 2011 *Proc. E-MRS 2011 Fall meeting: Symp. K (Warsaw University of Technology, Poland, 19-23 September 2011)* p. 32
- [25] Liewhiran C, Tamaekong N, Wisitsoraat A and Phanichphant S 2009 *Sensors* **9** 8996
- [26] Cukrov L M, McCormick P G, Galatsis K and Wlodarski W 2001 *Sensors and Actuators B* **77** 491
- [27] Korotcenkov G 2005 *Sensors and Actuators B* **170** 209
- [28] Lu F., Liu Y, Dong M and Wang X 2000 *Sensors and Actuators B* **66** 225